Multimodal Imaging Features and Clinical Relevance of Subretinal Lipid Globules

PEDRO FERNÁNDEZ-AVELLANEDA, K. BAILEY FREUND, REEKING K. WANG, QINGHUA HE, QINQIN ZHANG, SERENA FRAGIOTTA, XIAOYU XU, GERARDO LEDESMA-GIL, YOSHIMI SUGIURA, MARK P. BREAZZANO, LAWRENCE A. YANNUZZI, SANDRA LIAKOPOULOS, DAVID SARRAF, AND ROSA DOLZ-MARCO

• PURPOSE: To describe the presence of subretinal lipid globules (SLG), analyze the multimodal imaging features inherent in their optical properties, and provide a means to distinguish them from other retinal structures and clinical signs.

• DESIGN: Retrospective cohort study.

• METHODS: The clinical data and multimodal imaging features of 39 patients (49 eyes) showing SLG were evaluated. Patients underwent color fundus photography, near-infrared reflectance (NIR), spectral-domain (SD) and swept-source (SS) optical coherence tomography (OCT) and OCT angiography. In vitro phantom models were used to model OCT optical properties of water, mineral oil, and intralipid droplets and to investigate the optical mechanisms producing hypertransmission tails beneath SLG.

• RESULTS: The SLG were not visible in color fundus photographs or in NIR images. With both SD- and SS-OCT B-scans, SLG appeared as 31-157 μm, round, hyporeflective structures demonstrating a characteristic hypertransmission tail previously described with lipid globules found in the choroid and in neovascular membranes. Similarly, with en face OCT, SLG appeared as small, round, hyporeflective structures. SLG were encountered most often in eyes with neovascular age-related macular degeneration (AMD) that had type 1 macular neovascularization (MNV) (91.1%). Of those eyes, 93.3% were receiving intravitreal antivascular endothelial growth factor (VEGF) therapy (median of 15 injections) with a mean follow-up of 52.6 months. The number of prior injections positively correlated with the number of SLG. The detection of MNV preceded the presence of SLG in 66.7% of cases. En face OCT showed that, in many eyes (49%), SLG appeared in clusters of >10. In 38.8% of eyes, SLG were found overlying type 1 MNV, and in 44.9% of eyes, often those with more numerous SLG, the SLG were located near the lesion border. In 2 eyes with AMD followed for nonexudative type 1 MNV, SLG were detected prior to the detection of other imaging signs of exudation. SLG were observed in several other exudative macular diseases. Phantom models demonstrated that the hypertransmission tail beneath SLG is related to a lensing effect produced by these hyporeflective spherical structures.

• CONCLUSIONS: SLG are a newly recognized OCT feature frequently seen in eyes receiving intravitreal anti-VEGF therapy for type 1 MNV due to AMD. OCT B-scans show SLG as small, round, hyporeflective structures with a characteristic hypertransmission tail. This OCT signature is influenced by the OCT focal plane, and it relates to reduced signal attenuation through oil and a lensing effect created by a higher refractive index compared to surrounding tissue. (Am J Ophthalmol 2021;222:112–125. © 2020 Elsevier Inc. All rights reserved.)

Accepted for publication Sep 1, 2020.

From the Vitreous Retina Macula Consultants of New York (P.F-A., K.B.F., M.P.B., L.A.Y.); Department of Ophthalmology (P.F-A., K.B.F., M.P.B., L.A.Y.), New York University Grossman School of Medicine, New York City, New York; Department of Ophthalmology (P.F-A.), Basurto University Hospital, Bilbao, SP; LuEsther T. Mertz Retinal Research Center (K.B.F., M.P.B., L.A.Y.), Manhattan Eye, Ear, and Throat Hospital; Harkness Eye Institute (K.B.F., M.P.B., L.A.Y.), Columbia University College of Physicians and Surgeons, New York City, New York; Department of Bioengineering (R.K.W., Q.H., Q.Z.), University of Washington, Seattle, Washington; Neuroscienze Salute Mentale e Organi di Senso Department (S.F.), Ophthalmology Unit, S. Andrea Hospital, University of Rome La Sapienza, Rome, IT; State Key Laboratory of Ophthalmology (X.X.), Zhongshan, CH; Ophthalmic Center (X.X.), Sun Yat-sen University, Guangzhou, CH; New York Eye and Ear Infirmary of Mount Sinai (G.L-G.), New York City, New York, USA; Department of Ophthalmology (Y.S.), Faculty of Medicine, University of Tsukuba, JA; Department of Ophthalmology (S.L.), Faculty of Medicine and University Hospital Cologne, GM; Stein Eye Institute (D.S.), University of California, Los Angeles, Los Angeles, California; Unit of Macula (R.D-M.), Oftalvist Clinic, Valencia, SP, USA.

Inquiries to K. Bailey Freund, Vitreous Retina Macula Consultants of New York, 950 Third Ave, New York, NY 10022, USA; e-mail: kbfnyf@aol.com

LIPIDS ARE BIOMOLECULES CHARACTERIZED BY THEIR solubility in nonpolar organic solvents and insolubility in water. Lipids are essential structural components of cell membranes; they play key roles in normal retinal function and provide energy. In those roles, they are vital for neuronal transmission and metabolic activities. Lipid distribution in the retina varies according to retinal topography (macula or peripheral retina) and patient age.[1,2]

In 1966, Friedman and Smith[3] described lipid globules within the anterior choroid of both normal eyes and eyes with various retinal diseases by using light microscopy and special staining methods. More recently, Querques and associates[4] proposed the term "choroidal cavern" to

0002-9394/$36.00
https://doi.org/10.1016/j.ajo.2020.09.003

describe an optical coherence tomography (OCT) finding within the choroid of eyes with geographic atrophy due to age-related macular degeneration (AMD).[4] The choroidal caverns appeared as hyporeflective round structures without a hyper-reflective border in areas devoid of vessels. Indocyanine green angiography and OCT angiography (OCTA) failed to show vascular flow within these lesions. The authors suggested that these structures may correspond to "ghost vessels" previously described by Mullins and associates[5] and Biesemeier and associates.[6] Dolz-Marco and associates,[7] reported similar hyporeflective OCT structures in eyes with a wider range of diagnoses, which included not only geographic atrophy but neovascular AMD, central serous chorioretinopathy, and in apparently normal eyes of healthy patients.[7] These structures, identified in both the choroid and the sub-retinal pigment epithelium (sub-RPE) space, showed a characteristic hypertransmission tail on OCT B-scans. Based on a histological analysis of lipid globules in eyes of human donors and multimodal imaging characteristics of choroidal and sub-RPE caverns in vivo, the authors hypothesized that choroidal and sub-RPE caverns were lipid-rich structures, likely the OCT equivalent of the lipid globules previously described by Friedman.[7]

This study investigated the multimodal imaging features of similar hyporeflective structures believed to represent small spherical lipid globules found in the subretinal space. The optical properties of lipid producing a characteristic OCT hypertransmission tail in both these lesions and choroidal and sub-RPE lipid globules were modeled in 2 in vitro phantom experiments. Based on this study's findings, the term "subretinal lipid globules (SLG)" was originated for this new finding, and the relationship between the appearance of SLG and the timing of anti-VEGF injections as a clinical surrogate for exudation were explored.

METHODS

THIS STUDY FOLLOWED THE TENETS OF THE DECLARATION of Helsinki, and complied with the Health Insurance Portability and Accountability Act of 1996, and was approved by the Western Institutional Review Board (Olympia, WA, USA). Written informed consent was obtained from all participants. Participants in this study were recruited from volunteers who agreed to be examined and met the eligibility criteria described below at the Vitreous Retina Macula Consultants of New York (New York, NY, USA) between July 2017 and January 2019.

• **PARTICIPANTS:** This was a retrospective review of the clinical and multimodal imaging data from patients with SLG detected on cross-sectional optical coherence tomography (OCT). All patients were seen in the offices of the Vitreous Macula Consultants of New York. Patients were included if spectral domain (SD)-OCT B-scans showed SLG appearing as small, round, hyporeflective lesions in the subretinal space with a characteristic tail of posterior hypertransmission. Additionally, all SLG showed the following imaging characteristics previously described for lipid globules found in other retinal tissues[7]: 1) color fundus photographs (CFP) were not visible; 2) fundus autofluorescence (FAF) was isoautofluorescent; 3) near infrared reflectance (NIR) was isoreflective; 4) en face OCT with SLG included within the segmentation boundaries were round, hyporeflective lesions; 5) en face OCT with segmentation boundaries positioned posterior to the SLG within their hypertransmission tails showed round areas of relative hyperreflectivity; and 6) en face OCTA appeared as an absent flow signal.

For each patient, demographic information, including age, sex, and race, was obtained from their electronic health record. Information regarding best-corrected visual acuity (BCVA) and ocular and medical comorbidities were also obtained (blood pressure, dyslipidemia, diabetes, smoking habit; medication usage, including statins; and cardiovascular events).

In eyes for which longitudinally tracked SD-OCT was available, following the first detection of SLG, all prior and subsequent SD-OCT volumes were analyzed. In order to classify SLG as static or dynamic structures, a longitudinal evaluation for the presence and location of SLG was performed for each numbered OCT B-scan within the tracked SD-OCT volumes. The temporal relationship between the presence of SLG and concomitant exudative AMD findings was analyzed. For this analysis, exudation in the context of neovascular AMD was defined as subretinal and/or intraretinal fluid present on OCT and judged to be due to MNV with or without associated hemorrhage or clinically visible lipid. The MNV lesion type and the characteristics of the treatment with intravitreal antivascular endothelial growth factor (VEGF) therapy (drug used and number of injections) were recorded. When classifying SLGs according to location overlying or at the border of the MNV lesion, the B-scan from the first visit, when both SLG and MNV were identified, was used. En face OCT was used to verify SLG location with respect to MNV.

• **MULTIMODAL IMAGING:** All eyes with SLGs were imaged using CFP, FAF, NIR, and SD -OCT. Most eyes had also been imaged with en face swept source (SS)-OCT and en face SS-OCT angiography (OCTA). Color images were recorded using the TRC-50DX fundus camera (Topcon Medical Systems, Paramus, NJ, USA) and the Eidon confocal true color fundus camera (Centervue, Padova, IT). Long-wavelength FAF images were acquired using the TRC-50DX fundus camera (Topcon) using a conventional halogen lamp, a 580-nm band-pass filter (bandwidth, 500-610 nm), and a barrier filter of 695 nm (bandwidth, 675-715 nm). Short-wavelength autofluorescence, NIR, and SD-OCT images were obtained using a

TABLE 1. Summary of Clinical and Demographic Characteristics for the Present Cohort

Variables	Data
Number of patients	39
Number of eyes	49
Females	18 (46.2)
Whites	37 (94.4)
Bilateral	10 (28.6)
Medical history	
Hypertension	23 (59)
Hypercholesterolemia	16 (41)
Diabetes	4 (10.3)
Statin use	13 (33.3)
Smoking	14 (35.9)
Systemic comorbidities	
Cardiovascular disease	11 (28.2)
Cancer	8 (20.5)
Thyroid disease	5 (12.8)
Stroke/TIA	3 (8.6)
Osteoporosis	2 (7.7)
IBD	2 (5.1)
PKD	1 (2.6)

BCVA = best-corrected visual acuity; IBD = inflammatory bowel disease; logMAR = logarithm of the minimum angle of resolution; PKD = polycystic kidney disease; TIA = transient ischemic attack.

Data are presented as: Number (%).

Spectralis HRA-OCT machine (Heidelberg Engineering, Erlangen, GM). The raster scanning protocols used were both "fast" 25 B-scans, each consisting of 512 A-scans and "dense" 1,024 A-scans ×49 B-scans. In all cases, OCT scans were eye-tracked with follow-up mode activated. For SS-OCT and en face SS-OCT, en face SS-OCTA images and flow B-scans Plex Elite 9000 (Carl Zeiss Meditec, Dublin, California, USA) were used. Acquisition protocols of 3 × 3- or 6 × 6-mm volume cubes were used.

• **LIPID GLOBULES PHANTOM EXPERIMENT:** Two separate in vitro phantom experiments were performed. The first explored relationships between globule size and the optical properties of materials. Two different tube sizes were used: a tube with an inner diameter of 375 (large) and one with a 50-μm (small) diameter. Those tubes were filled with 3 different materials. Water was used to simulate fluid, mineral oil to simulate lipid globules, and a 20% intralipid solution (flowing scattering particles) to simulate blood within vessels, whereas titanium dioxide (TiO_2) 0.3% was used as the background scattering. An SD-OCT scan was performed in the lumens of the tubes to see the behavior of the different materials inside. For SD-OCT, a 1,340-nm central wavelength and a 92- kHz scan rate were used.[8] The scanning pattern consisted of 400 A-line × 400 B-scan × 8 repetition. The second experiment was performed in order to demonstrate the relationship between the refractive index (RI) of oil and a lensing effect seen on OCT B-scans.[9,10] Various oil types were tried. Olive oil, clove oil, and cinnamon oil were dispersed in a scattering agar gel phantom that was stirred until the agar jelled. Olive oil has an RI range of 1.44-1.47. Cinnamon oil has an RI range of 1.59-1.62. The average RI of retinal tissue is approximately 1.38. SD-OCT imaging was performed using different focal planes.

• **STATISTICAL ANALYSIS:** The quantitative variables were expressed as mean ± standard deviation. In the case of non-normal distribution, means were reported with 95% confidence intervals (CI). Logarithm minimal angle of resolution (logMAR) visual acuity was calculated using the procedure outlined by Holladay.[11] The distribution normality was verified using the Shapiro-Wilk normality test. The χ^2 test was used to compare categorical variables, whereas the paired *t*-test was used to assess differences between 2 time points. The Spearman rank correlation or Kendall tau coefficient were calculated to determine the relationship between ordinal variables. *P* values less than .05 were considered statistically significant, and $P < .001$ was highly statistically significant. All calculations were carried out using SPSS version 20 software (SPSS, Chicago, Illinois, USA).

RESULTS

A TOTAL OF 49 EYES OF 39 PATIENTS AT A MEAN 75.1 ± 9.2 years of age met inclusion criteria. A total of 94.4% of the patients were white, and 46.2% were female. In 28.6% of cases, SLG were bilateral. BCVA at the baseline visit was 0.29 ± 0.2 logMAR (median, 0.3; Snellen equivalent, 20/40). Mean duration of follow-up until SLG appearance was 2.8 years (95% CI, 1.9-3.8; median, 2 years). At the most recent examination, BCVA was 0.3 ± 0.25 logMAR (median, 0.3; Snellen equivalent, 20/40). Differences between BCVA at first and last visits were not significant (paired *t*-test, $P = .51$). Demographic data are shown in Table 1.

• **MULTIMODAL IMAGING FEATURES OF SUBRETINAL LIPID GLOBULES:** SLG were not visible on CFPs, FAF, or NIR. On SD-OCT B-scans, SLG appeared as well-delineated, round, hyporeflective structures measuring 31-157 μm. SLGs were always identified between the ellipsoid zone (EZ) and the RPE/Bruch membrane complex. A characteristic hypertransmission tail was detected in all cases (100%).

En face SS-OCT was available for 42 eyes with SLG (85.7%) (Figure 1). A custom-segmented slab of the EZ + interdigitation zone (IZ) using "RPE-fit" as the upper

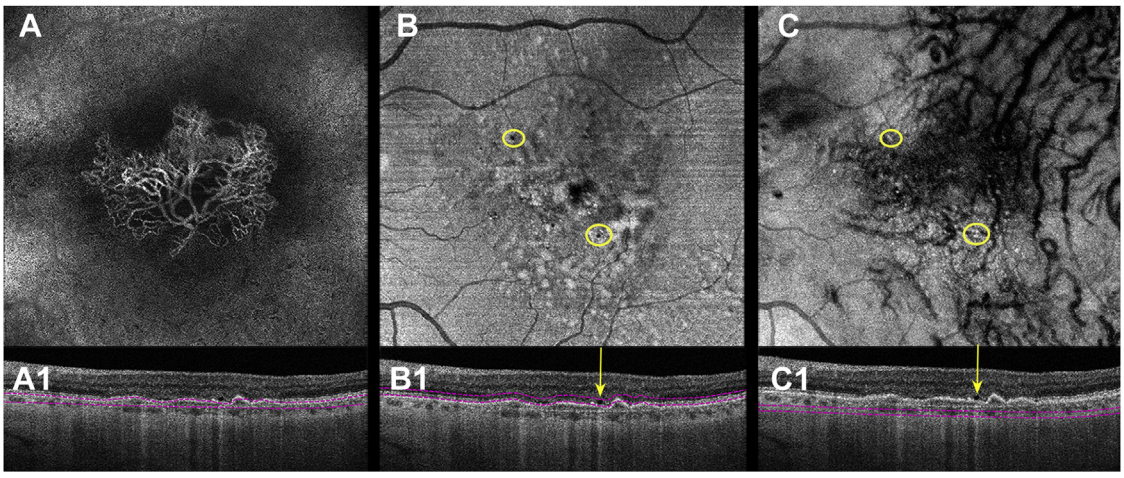

FIGURE 1. Multimodal imaging characteristics of SLG in an eye with type 1 MNV due to age-related macular degeneration. (A) A 6 × 6-mm en face OCT angiogram shows type 1 MNV. (B) A 6 × 6-mm en face OCT projection showing hyporeflective SLG (yellow circles) in the subretinal space. (C) A 6 × 6-mm en face OCT projection showing hyper-reflective round areas (yellow circles) representing the hypertransmission tails each SLG. The purple dashed lines in A1, B1, and C1 indicate the segmentation boundaries used for the corresponding en face projections. MNV = macular neovascularization; OCT = optical coherence tomography; SLG = subretinal lipid globules.

and lower segmentation boundaries revealed the SLG to be hyporeflective circular spots in 41 eyes (97.6%), whereas adjustment of the slab through the sclerochoroidal junction beneath the SLG demonstrated hyper-reflective circular spots corresponding to their hypertransmission tails (41 eyes, 97.6%). Neither en face OCTA nor OCTA B-scans demonstrated flow signal within the SLG.

The number of SLG detected with en face OCT was greater than 10 in nearly half the cases (24 cases, 49%), as reported in Table 2, which summarizes the main topographic findings. The occurrences of new SLGs were identified overlying and at the borders of the MNV lesions ($r = 0.53$; $P < .001$). The occurrence of SLG as clusters was related to an increasing number of SLG ($r = 0.42$; $P = .003$). Longer MNV follow-up after diagnosis was associated with SLG located overlying and at the border of the MNV lesion ($r = 0.33$; $P = .02$). Area measurements of individual SLG were less than <0.01 mm^2 and could not be accurately measured.

TABLE 2. Topographic Features of SLG with Spectral-Domain or Swept-Source OCT B-Scans and Swept-Source en face OCT

Characteristics	Subjects (n = 44 eyes)
Number of SLG	
>10	24 (49)
6-10	10 (20.4)
2-5	10 (20.4)
1	5 (10.2)
Distribution	
Cluster	35 (71.4)
Diffuse	14 (28.6)
Location with respect to MNV	
Overlying	19 (38.8)
Marginal	8 (16.3)
Both	22 (44.9)

MNV = macular neovascularization; OCT = optical coherence tomography; SLG = subretinal lipid globules.
Values are numbers (%).

• **CLINICAL ASSOCIATIONS OF SUBRETINAL LIPID GLOBULES:** The majority of eyes (45 eyes, 92% of patients) had MNV lesions secondary to AMD. In 4 eyes with SLG (8.0%) multimodal imaging showed no evidence of MNV lesions including 1 eye (2.0%) with central serous chorioretinopathy (Figure 2), 1 eye (2.0%) with a choroidal hemangioma (Figure 3), and 2 eyes (4.0%) with nonexudative atrophic AMD. In the eyes with neovascular AMD, 41 (91.1%) had type 1 MNV lesions (Table 3), 3 aneurysmal (polypoidal) type 1 MNV (6.7%), and 1 type 2 MNV lesion (2.2%). MNV lesions appeared prior to the appearance of SLG in 30 eyes (66.7%), within a mean of 24 months (95% CI, 10.7-37.2) from the onset of treatment to the first detection of SLG. In 13 eyes (28.9%), SLG were detected at the same visit as when MNV was observed. Only in 2 eyes (4.4%) were SLG detected prior to the MNV lesion. A treat and extend regimen (TER) protocol was used in 42 of 45 eyes (93.3%) with MNV lesions, and of those eyes, 41 eyes (97.61%) showed evanescence of SLG after intravitreal therapy on cross-sectional SD-OCT. The mean total follow-up for those cases was 52.6 months (95% CI: 40.5-

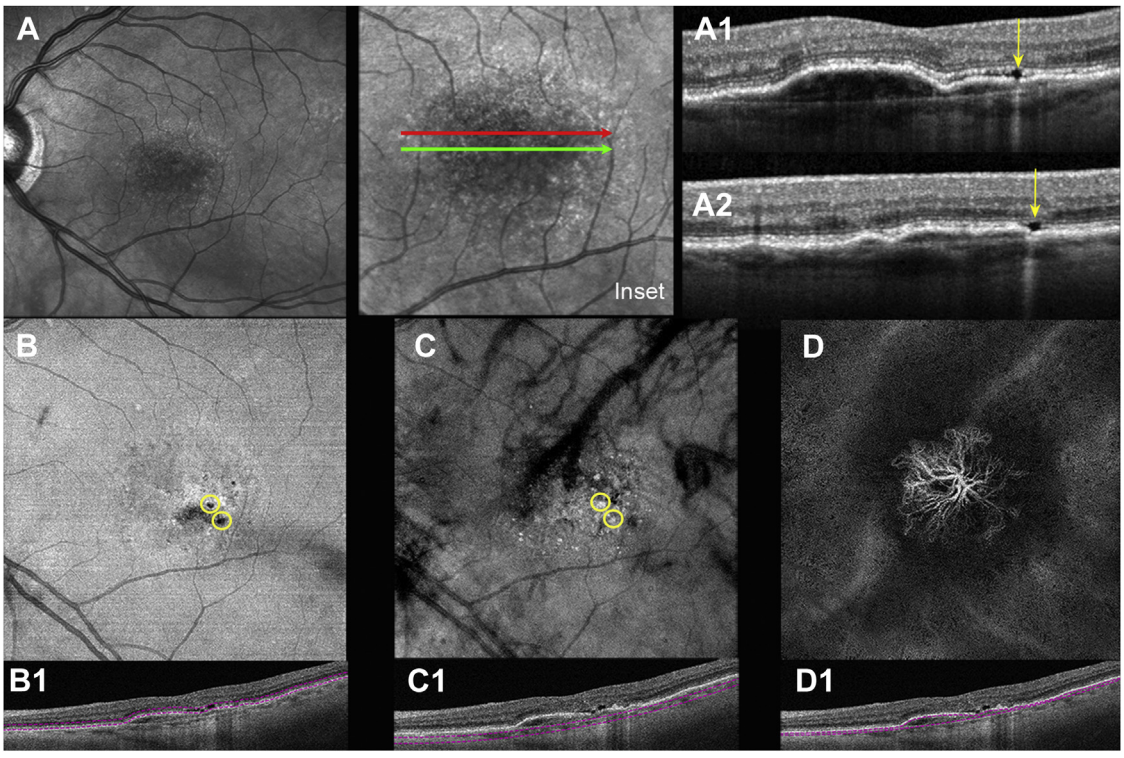

FIGURE 2. Multimodal imaging characteristics of SLG in an eye with type 1 MNV due to neovascular age-related macular degeneration AND pachychoroid disease features. (A) Near-infrared reflectance image with an expanded image (inset). (A1) SD-OCT B-scan corresponding to the red arrow. (A2) OCT B-scan corresponding to the green arrow. (A1 and A2) show hyporeflective SLG with characteristic hyper-reflective tails. (B) A 6 × 6-mm en face OCT projection of the outer retina (purple dashed lines [B1]) shows the SLG as hyporeflective round lesions (yellow circles). (C) A 6 × 6-mm en face OCT projection of the choroid (purple dashed lines [C1]) shows hyper-reflective round areas (yellow circle) representing the hypertransmission tails of the overlying SLG. (D) A 6 × 6-mm en face OCT angiography projection (purple dashed lines [D1]) shows flow signal within type 1 macular neovascularization. MNV = macular neovascularization; SD-OCT = spectral-domain optical coherence tomography; SLG = subretinal lipid globules.

64.7; median, 43 months), with a mean cumulative number of 23 injections (95% CI: 16.04-30.03; median, 15 injections). Intravitreal aflibercept (2.0 mg/0.05 ml) was used in 28 treated eyes (66.7%), whereas 14 eyes (33.3%) initiated treatment with ranibizumab (0.5 mg/0.05 ml), and were switched to aflibercept (2.0 mg/0.05 ml) during the follow-up period. The cumulative number of SLG correlated with the total number of anti-VEGF injections ($r = 0.43$; $P = .002$). SLG were observed in 2 eyes (4%) with untreated type 1 MNV due to AMD (identified with SS-OCTA) that lacked any other findings of exudation (Figure 4). In those 2 eyes, more typical signs of exudation occurred at 31 months and 92 months after the first detection of SLG.

• **LIPID GLOBULES PHANTOM EXPERIMENT:** The first experiment (Figure 5) used the large tube size (375 μm inner diameter). The signal below 20% intralipid was attenuated, and a flow artifact was detected (suspended scattering particles in motion),[12] whereas in the case of water and mineral oil, the signal below was enhanced compared to the background tissue at the same level, and no flow artifact was observed. After the tube with the 50-μm inner diameter was used, both water and intralipid showed an increased signal below. However, in the case of water, hypertransmission of the underlying OCT signal was observed, which was different from the projection artifacts caused by intralipid scattering solution. One important limitation was found due to the surface tension; it was difficult if not impossible to introduce mineral oil into the small tube with the current facilities. This is why only water was used at the time of filling 50-μm diameter tubes.

In the second experiment (Figure 6), the transparent aggregates formed by accumulation of oils (oil droplets) were used. Their RI (>1.44) was higher than that of the surrounding tissue (~1.38). When imaged by OCT, they were hyporeflective (dark, looking like a "cavity"). However, such droplets can cause a lensing effect in OCT imaging. Accordingly, this lensing effect was dependent on the position of the oil droplet relative to the OCT focal plane. Above the OCT focal plane, the oil droplet strengthened the focus, shortened the effective OCT focal length, and led to a short and highly reflective tail below the droplet

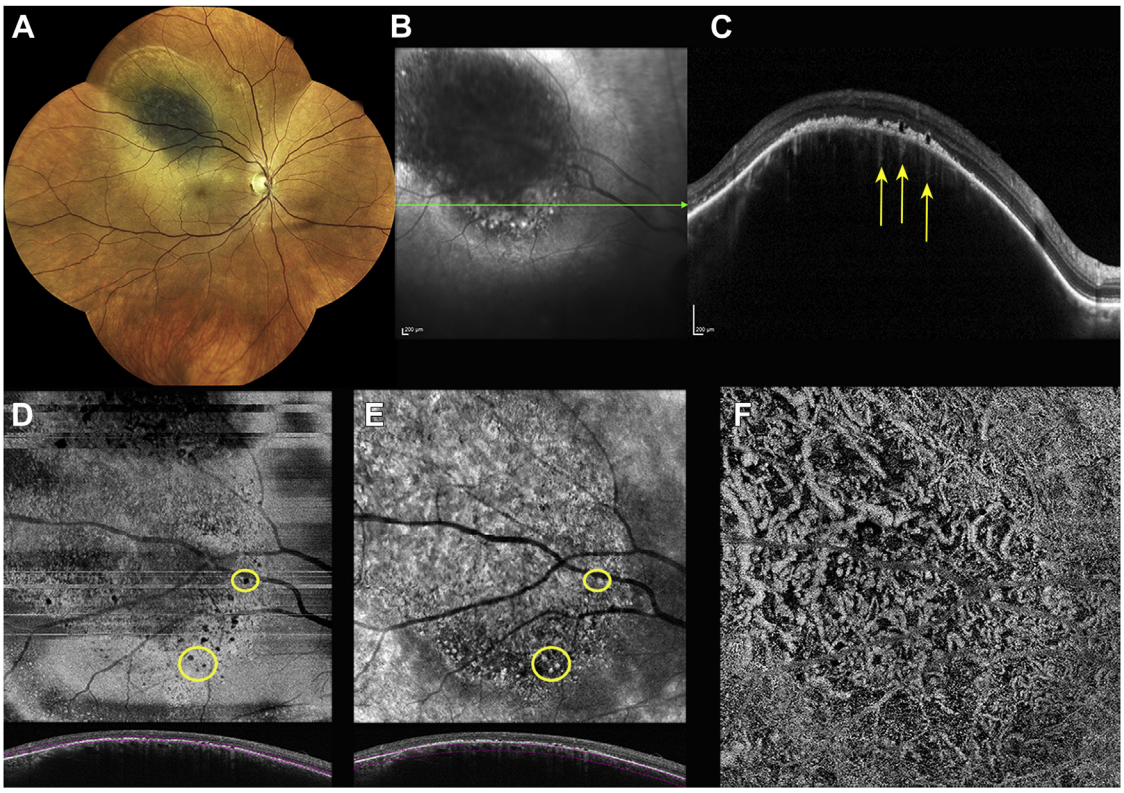

FIGURE 3. SLG in an eye with a circumscribed choroidal hemangioma. (A) Color confocal true color montage image shows a choroidal hemangioma with surrounding subretinal exudation. (B) Near-infrared reflectance image with a green arrow indicating the location and direction of the swept-source optical coherence tomography (SS-OCT) B-scan shown in (C). SS-OCT shows multiple hyporeflective round SLG with the characteristic hyper-reflective tails (yellow arrows) near the border of exudation at the inferior margin of the tumor. (D) A 6 × 6-mm en face OCT projection of the outer retina (purple dashed lines (D1) shows the SLG as hyporeflective round lesions (yellow circles). (E) A 6 × 6-mm en face OCT projection of the inner choroid (purple dashed lines [D1]) shows hyper-reflective round areas (yellow circles) representing the hypertransmission tails of the overlying SLG. (F) A 6 × 6-mm en face OCT angiography projection of the deeper choroid (segmentation lines not shown) shows a "bag of worms" pattern of flow signal within the vascular tumor. SLG = subretinal lipid globules; SS-OCT = swept-source optical coherence tomography.

(stronger OCT reflectance). At the OCT focal plane, there was not a significant effect. Below the OCT focal plane, the oil droplet will refocus the defocused light and form a long tail, with reflections stronger than the surrounding tissue. This focal plane reflection could be compared to RPE.

DISCUSSION

TO THE AUTHORS' KNOWLEDGE, THIS IS THE FIRST CLINICAL description of lipid globules in the subretinal space, referred to here as "subretinal lipid globules" (SLG). Multimodal imaging showed that SLG demonstrated imaging features similar to lipid globules described previously in the choroid, sclera, and associated with type 1 MNV lesions (Figure 7).[7] These clinical observations are supported by in vitro OCT and OCTA phantom experiment results.

Hyporeflective spaces in the choroid imaged with OCT, first described by Querques and associates as choroidal caverns,[4] were thought to represent sclerotic vessels or "ghost vessels." Based on an indirect correlation of in vivo clinical imaging with the ex vivo histologic data from 2 independent case series of donor eyes, Dolz-Marco and associates

TABLE 3. Macular Neovascularization Subtypes Accompanying the Presence of Subretinal Lipid Globules

MNV Subtypes	Subjects (n = 45 eyes)
Type 1	41 (91.1)
PCV/AT-1	3 (6.7)
Type 2	1 (2.2)

MNV = macular neovascularization; PCV/AT-1 = polypoidal choroidal vasculopathy/aneurysmal type 1 macular neovascularization.
Values are number (%).

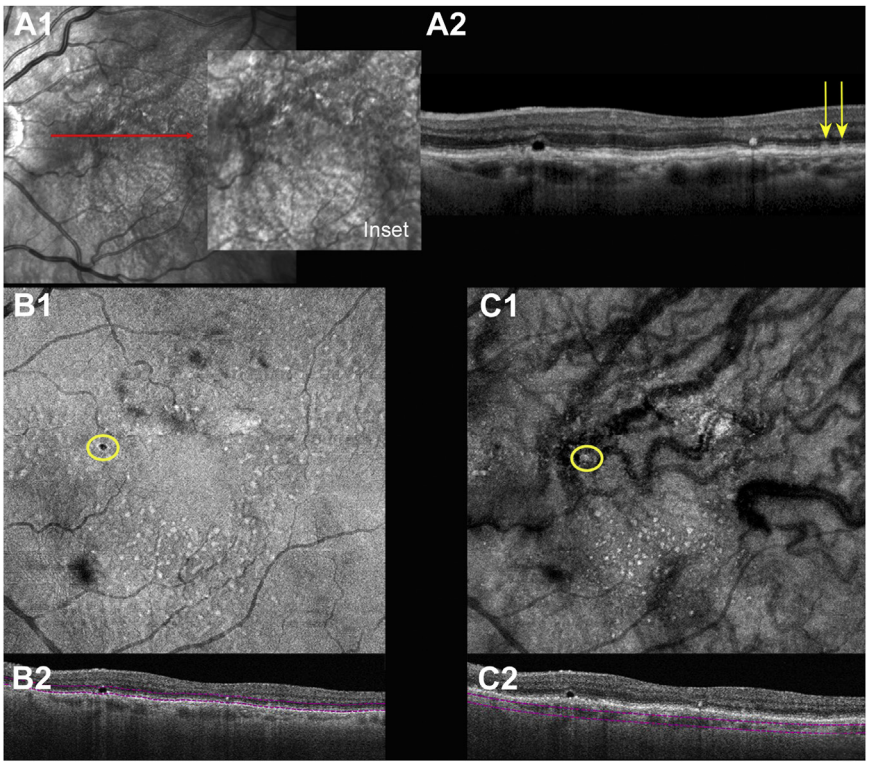

FIGURE 4. Subretinal lipid globules in an eye with non-exudative neovascular age-related macular degeneration and SDD. (A1) Near-infrared reflectance image with an expanded image (inset) showing characteristic hyporeflective target lesions corresponding to SDD. (A2) Spectral-domain OCT shows a round hyporeflective subretinal lipid globule with a hypertransmission tail overlying a shallow retinal pigment epithelium elevation harboring nonexudative type 1 macular neovascularization. Yellow arrows indicate SDD. (B1) A 6 × 6-mm en face OCT projection with segmentation of the outer retina (purple dashed lines [B2]) shows the hyporeflective subretinal lipid globule (yellow circle). (C1) A 6 × 6-mm en face OCT projection with segmentation of the deep choroid (purple dashed lines [C2]) demonstrates a hyper-reflective round area (yellow circle) representing the hypertransmission tail of the overlying SLG in B1. OCT = optical coherence tomography; SDD = subretinal drusenoid deposits.

proposed that choroidal caverns are lipid rich dynamic structures[7] representing the OCT signature of the choroidal lipid globules first described by Freidman and Smith in 1966.[3] Findings from this study show similar hyporeflective spherical lesions in the subretinal space sharing similar imaging features of lipid globules found in other ocular tissues. Although choroidal caverns likely represent choroidal lipid globules, SLG are found in a different anatomic compartment, have a narrower range in size, a more consistent spherical shape, and more transient nature than choroidal caverns.

A comprehensive analysis of multimodal imaging was performed which demonstrated that, similar to sub-RPE and choroidal lipid globules, SLG were not detected with routine color fundus photography, NIR, and FAF.[7] As with lipid globules elsewhere, SD-OCT B-scans displayed SLG as round hyporeflective structures with a characteristic tail of hypertransmission. In all eyes, the area of individual SLG was <0.01 mm^2, the lower limit of detection for the OCT devices used in this analysis. These small area measurements are consistent with data previously reported by Friedman and Smith[3] and by Dolz-Marco and associates.[7] With OCT, hyper-reflective dots were rarely noted in association with SLG indicating an absence of inflammation, which is consistent with the histologic findings of sub-RPE and choroidal lipid globules.[7] In most cases, a cluster of ≥10 SLG was identified overlying or contiguous with type 1 MNV lesions. En face OCT images illustrated the optical properties of SLG. Using a custom segmentation of the EZ and IZ, these spherical structures displayed small hyporeflective circular areas with en face projection and hyperreflectivity when the segmentation was displaced more posterior, closer to the sclerochoroidal junction, due to the capture of the hypertransmission tail posterior to each lesion.

The origin of OCT reflectivity occurs at interfaces between materials of different refractive indexes.[7,13] The optical properties of any structure relate to its size, shape, and refractive index, and to the scanning wavelength parameters. Particle size influences OCT behavior. Particles with smaller diameter enhance light transmission leading to greater signal penetration or "hypertransmission." Hypertransmission can also relate to a lensing effect from small

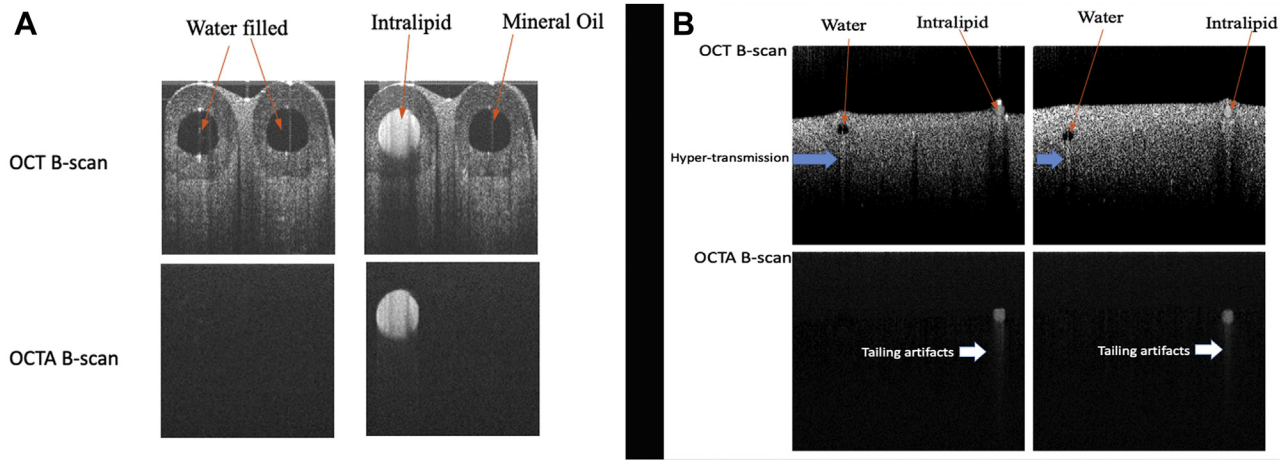

FIGURE 5. Phantom OCT and OCTA experiment using water, mineral oil (simulating subretinal lipid globules), and 20 % intralipid (simulating blood) to demonstrate optical properties related to particle size. (A) Large tube (375-μm inner diameter). OCT B-scans using a 1,340 nm wavelength light through a large lumen filled with the 3 different materials. The structural OCT-B scan signal (top panels) below water and mineral oil are enhanced (hypertransmission) compared to the background tissue at the same depth level. With OCTA (bottom panels), a flow artifact is observed with intralipid due to SSPiM that is not seen with water or mineral oil. (B) Small tube (50-μm inner diameter). Similar findings were observed, but the surface tension of mineral oil precluded its introduction into the smaller tubes. OCT = optical coherence tomography; OCTA = optical coherence tomography angiography; SSPiM = suspended small particles in motion.

optically clear particles (globules or droplets)[14] with a spherical shape. Boschi and associates[15] studied the optical properties of lipid droplets and concluded that their spherical geometry and homogenous content reduced light absorption and scattering, resulting in low light dispersion. The refractive index of any substance relative to its surrounding medium influences light scattering in ocular tissues. This variable relates to the absorption properties of the material being scanned. Water and lipid enable ample transmission of light due to low absorption coefficients compared to blood.[7,13] Differences in scanning light wavelength also influence optical properties resulting in variability according to the OCT device. Light attenuation due to absorption may be negligible in SLG using wavelengths of 840, 1,060, or 1,310 nm. Light attenuation surrounding lipid globules is strong. In addition, the hyporeflective nature of globules facilitates the passage of light. The combined effect of the optical features described above results in the posterior hypertransmission tail seen below SLG. This posterior hyperreflectivity is more pronounced with SD-OCT (center wavelength: 840 nm) versus SS-OCT (center wavelength: 1,060 nm) devices, as scattering strength of tissue and blood is much greater with the former. The longer wavelength of SS-OCT, however, results in greater forward scattering than the shorter wavelength of SD-OCT. Therefore, projection artifacts occurring with SS-OCTA are more evident than with SD-OCTA. However, projection artifacts are also dependent on the backscattering by posteriorly located tissue, and SS-OCTA has weaker backscattering than the SD-OCT.

In order to demonstrate how optical properties related to tissue composition can influence the appearance of hypertransmission tails posterior to SLG, 2 phantom experiments were performed. The first experiment was intended to show the influence of particle properties on optical display. As surface tension prevented mineral oil from being introduced into the 50-μm tube, findings were based on the similar behavior of water and oil in larger tubes. A scanning wavelength of 1,310 nm was used, which has less scattering strength at the surrounding material as well as in blood. To address these limitations, a second experiment was performed to clarify parameters which could influence the appearance of hypertransmission tails posterior to SLG. Hyporeflective oils which have an RI of >1.45, higher than retinal tissue (RI = 1.38), created a lensing effect which was related to their position with respect to the OCT focal plane. Hypertransmission tails of oil droplets anterior to the focal plane were shorter and more intense, whereas those of oil droplets posterior to the focal plane were wider and less prominent (defocused).

The characteristic multimodal imaging properties of SLG, which were validated in the phantom experiments, provided essential information to differentiate hyporeflective SLG from other common hyporeflective subretinal structures such as the subretinal fluid (SRF) and outer retinal tubulation (ORT). While both SRF and the lumens of ORT appear hyporeflective on OCT, neither entity shows a prominent hypertransmission tail (Figure 8). Another subretinal finding potentially mistaken for SLG is refractile drusen

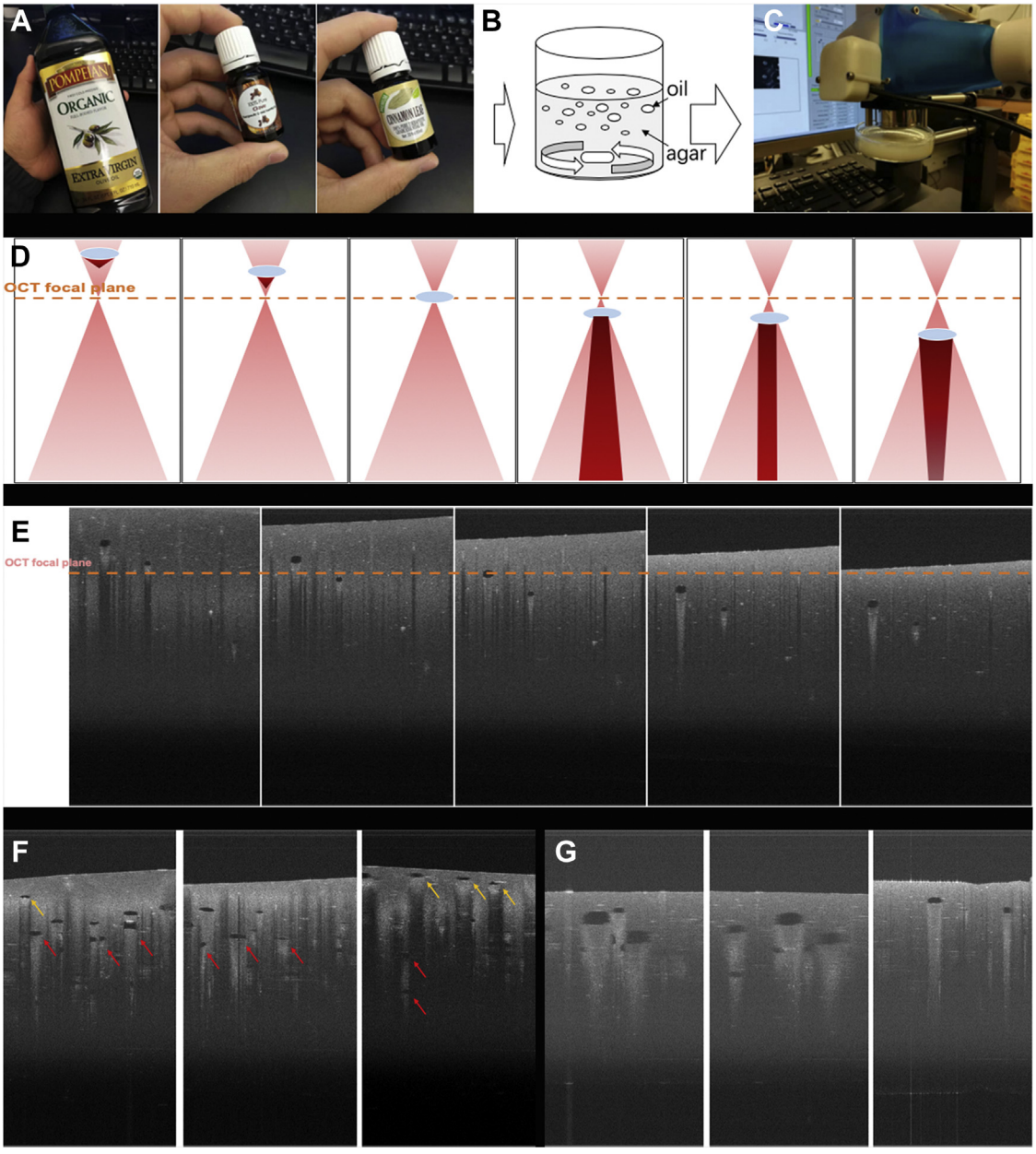

FIGURE 6. Phantom experiment to demonstrate lensing effects due to RI of oil as an explanation of the hyper-reflective tail posterior to SLG. (A) Transparent aggregates formed by accumulation of different oil-like materials (oil droplets) were used. (B) Olive, clove, and cinnamon oils were dispersed in a scattering agar-gel phantom by stirring before the agar jelled. (C) OCT was performed using different focal planes (D), supporting our hypothesis that, based on oil's hyporeflective content and RI (> 1.45) higher than retinal tissue's RI (1.38), a lensing effect should occur with OCT imaging. This lensing effect was dependent on the location of oil droplets with respect to the OCT focal plane. (E) If oil droplets were above the focal plane, they strengthened the focus and shortened the effective OCT focal length, leading to a short and highly reflective tail below the droplet (for stronger OCT reflectance, see yellow arrows in F). At the OCT focal plane, there was no significant lensing effect. Below the OCT focal plane, the oil droplets l refocused the defocused light, seen as a longer hypertransmission tail with stronger reflectivity than surrounding tissue (red arrows [F]). (G) Oil droplets showed the same optical behavior. OCT = optical coherence tomography; RI = refractive index; SLG = subretinal lipid globules.

containing hyporeflective cores composed of hydroxyapatite.[16] Although hypertransmission may also occur beneath refractile drusen due to overlying RPE and outer retinal atrophy, these lesions, unlike SLGs, are readily identified with color fundus photographs and NIR.

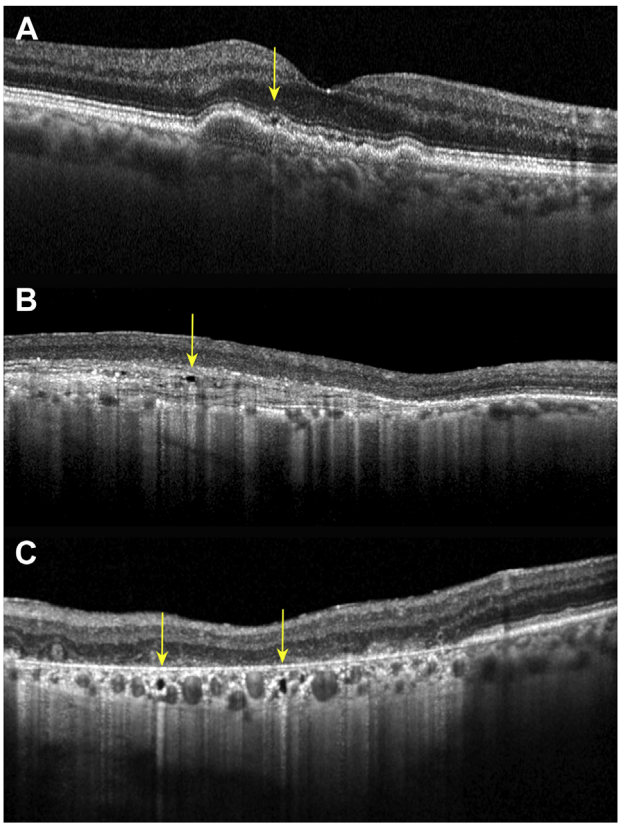

FIGURE 7. Optical coherence tomography B-scans show lipid globules with hypertransmission tails located in various ocular tissues. (A) Subretinal space (subretinal lipid globule). (B) Within type 1 macular neovascularization (lipid globule). (C) Within the choroid (choroidal cavern, Friedman lipid globule).

In this series, most eyes with SLG were receiving a TER regimen of intravitreal anti-VEGF therapy for type 1 MNV due to neovascular AMD. The SLGs were identified as overlying or near the margins of the type 1 lesions. Our data suggested that SLG may be associated with more mature lesions which often show large central vessels with smaller vessel loops near their margins on OCT.[17–19] The SLG in these eyes were dynamic lesions, reabsorbing and reappearing, often in the same area. In 2 eyes (4%) SLG were identified in association with type 1 MNV without any additional signs of exudation. The presence of type 1 MNV in eyes with nonexudative AMD has been confirmed with histopathologic studies and OCTA, and is referred to as nonexudative or quiescent MNV.[20–26]

New SLG in eyes with type 1 MNV treated with anti-VEGF therapy were often identified near the border of more mature lesions, with the number of SLGs increasing with the number of prior anti-VEGF injections. Sarks and associates[27] showed that the exudative component of MNV is not covered by pericytes in many eyes that received frequent intravitreal anti-VEGF injections. Reduced permeability due to pericytes is more likely to occur at the central mature vessels than in the more newly formed vessels near the lesion margin.[28] In some eyes, SLGs were observed to resolve following treatment and could recur in the absence of subretinal fluid (Figure 9). These authors hypothesized that SLG might have served as a biomarker of early disease activity[29]; however, the present methods could not confirm this potential and future study may explore the relationship of SLG and disease activity in neovascular AMD.

In the present cohort of eyes with AMD and SLGs, only 2 eyes had no evidence of MNV. Those eyes had various degrees of outer retinal atrophy (ORA) and RPE atrophy with ORA (RORA). The low prevalence of SLG in non-neovascular cases is not surprising; however, structural damage to the RPE and choroidal vessels, unrelated to angiogenesis, could occasionally lead to exudative or transudative OCT finds such as subretinal fluid and SLG. SLG were also detected in eyes with central serous chorioretinopathy (CSC) and choroidal hemangioma. In pachychoroid diseases, including CSC, choroidal vascular hyperpermeability (CVH), and compression of the inner choroidal by dilated Haller's layer vessels have been described.[30] Sakurada and associates[30] described multiple large choroidal lipid globules in eyes with pachychoroid diseases, with most found adjacent to pachyvessels in regions of CVH. Dysfunction of the RPE pump function helping to maintain the outer blood retinal barrier could contribute to both subretinal fluid and SLG present in some eyes with pachychoroid diseases.

Although the presence of SLG may represent a basic process of exudation, more complex mechanisms could also be involved. It has been reported that a lack of glucose and lipid at the level of the photoreceptors can induce a signal for neovascularization.[31] New vessels may proliferate in order to compensate for this relatively ischemic environment, leading to exudative complications. Lipoprotein lipase (LPL) is present in highly vascularized structures.[32,33] This molecule catalyzes the hydrolysis of plasma triglycerides to provide a greater supply of fatty acids to the photoreceptors when energy demands increase. These lipids can provide a source of energy to the photoreceptors and this process could contribute to an apparent protective effect of type 1 MNV.[34–36]

Limitations of this study include a retrospective design, relatively small sample size, and lack of data regarding the general prevalence of SLG in eyes with AMD or the other diagnoses in which they were identified. Furthermore, as a retrospective study of randomly chosen cases, there could be an ascertainment bias leading to the preferential selection of eyes with type 1 MNV lesions versus other lesion types. OCT caliper measurements of SLG was limited to the x and y axes, precluding SLG volume measurements. Moreover, the areas were reported as <0.01 mm,[2] which was at the lower limit of the OCT device. The number of

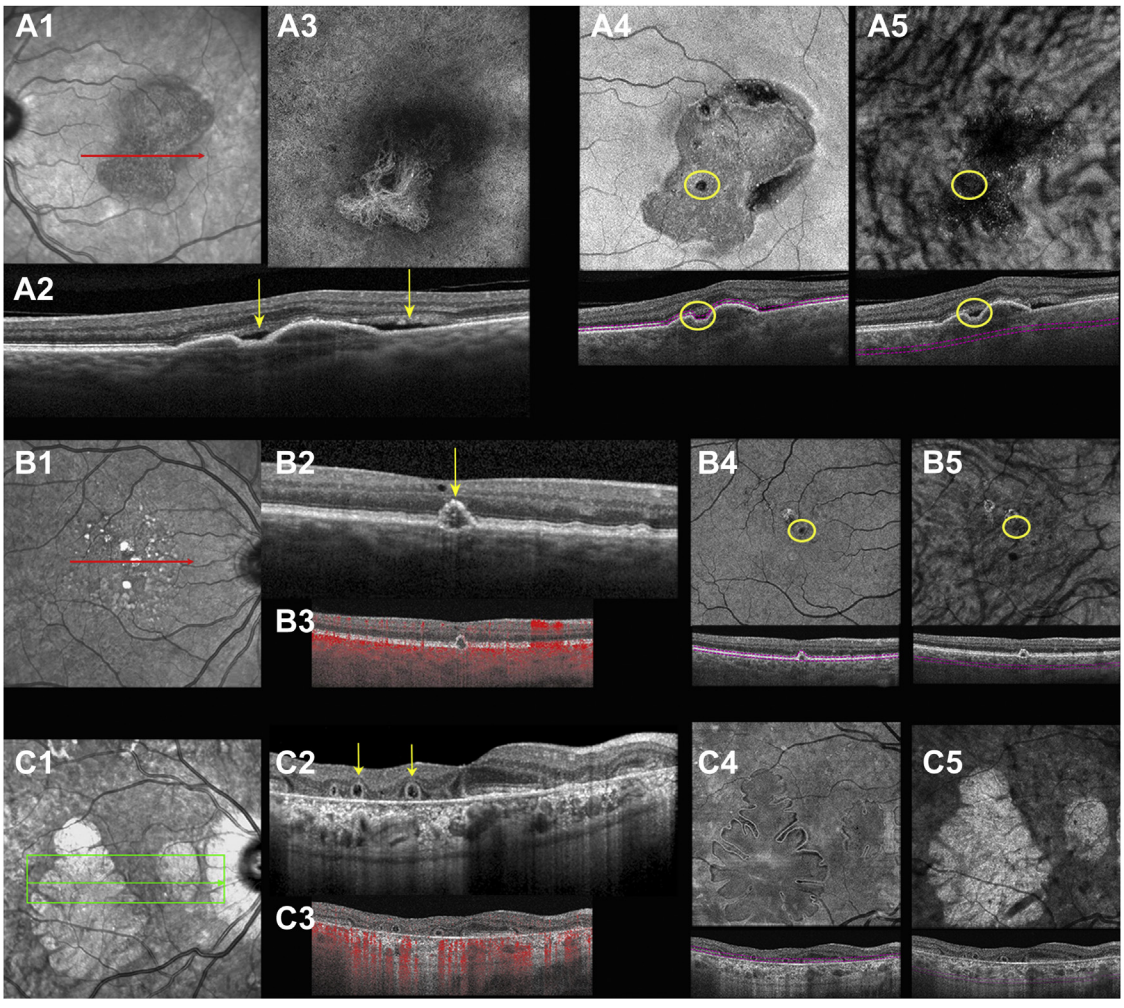

FIGURE 8. Distinguishing SLG from other hyporeflective subretinal materials. (A1-A5) Representative case demonstrating imaging characteristics of subretinal fluid. (A1) NIR with corresponding optical coherence tomography B-OCT scan (red arrow [A2]). Subretinal fluid is present (yellow arrows) due to the presence of type 1 macular neovascularization confirmed by en face OCTA (A3). En face OCT helps demonstrate the absence of a prominent hypertransmission tail as the hyporeflective area (yellow circle) seen with segmentation of the outer retina (A4) does not appear as a hyper-reflective area when the segmentation boundaries are moved into the choroid (A5). B1-B5. Representative case shows imaging characteristics of a calcified drusen. (B1) Red arrow in NIR shows the location and direction of the B-OCT scan shown in (B2). OCT B-scan shows a calcified drusen with a hyporeflective core composed of hydroxyapetite. A mild hypertransmission tail due to attenuation of outer retinal layers. (B3) OCT B-scan with flow signal overlay (red) shows no flow signal within the drusen. With en face OCT, the calcified drusen appears hyporeflective (yellow circle) with segmentation of the outer retina (B4) but does not appear as a hyper-reflective area when the segmentation boundaries are moved into the choroid (B5). C1-C5. Representative cases show imaging features of ORT. (C1) NIR reflectance shows ORT as well-defined finger-like extensions of relative hyporeflectivity into a large hyporeflective area of macular atrophy. (C2) OCT B-scan shows ORTs (yellow arrows) as round structures with hyporeflective lumens surrounded by hyper-reflective borders. The ORTs are located within the outer nuclear layer rather than the subretinal space. With en face OCT, ORTs appear as tubular structures with segmentation of the outer retina (C4). ORTs are not apparent when the segmentation boundaries are moved into the choroid (C5). NIR = near-infrared reflectance; OCTA = optical coherence angiography; ORT = outer retinal tubulation; SLG = subretinal lipid globules.

SLG identified with en face OCT analysis could vary with the device used (SD or SS), and only en face SS-OCT images were used in the present study. In the first phantom experiment, mineral oil could not be introduced into 50-μm tubes due to surface tension, and only a 1,310 nm wavelength light was used which produces less scattering of light by blood and the surrounding tissue. Although the second phantom experiment demonstrated that oil could reproduce the hyper-reflective tail which is related to a lensing effect due to its refractive index, a histopathological analysis will be required to validate the lipid composition of these hyporeflective round particles.

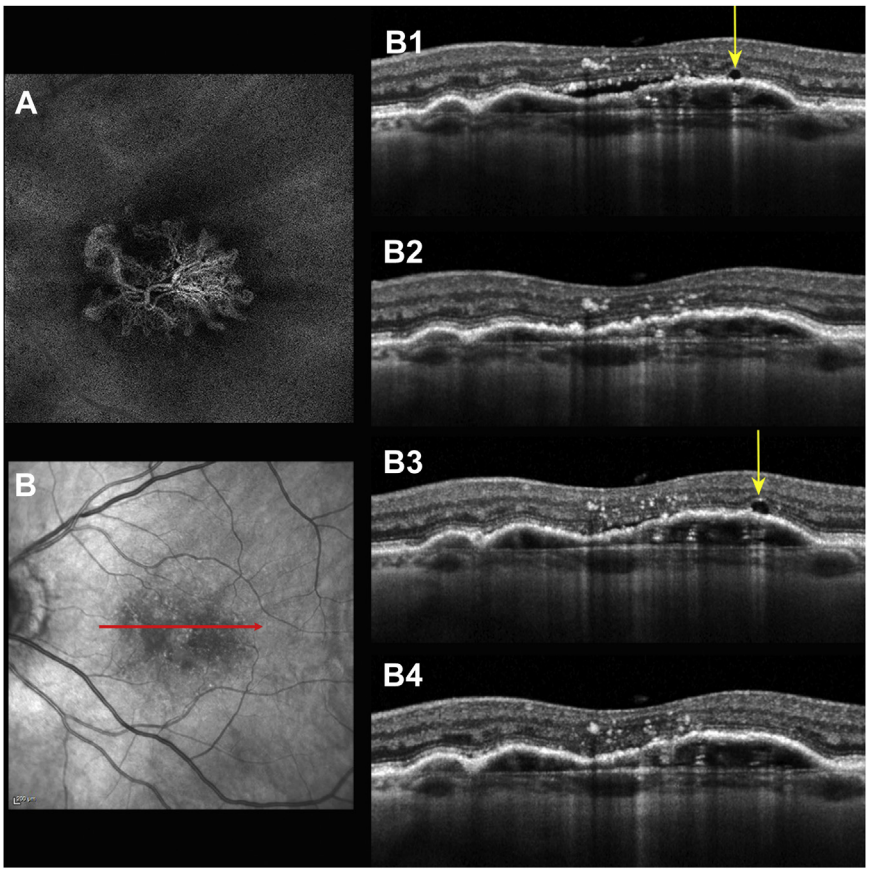

FIGURE 9. Representative case of type 1 MNV due to neovascular age-related macular degeneration associated with mild exudative changes managed with and intravitreal anti-vascular endothelial growth factor therapy on a treat-and-extend regimen. (A) A 6 × 6-mm en face optical coherence tomography angiography shows neovascular flow signal within subfoveal type 1 MNV. B. NIR of the same eye. (B1-B4) show eye-tracked B-OCT scans (corresponding to the red arrow in NIR) at various time intervals following treatment. Both SRF and SLGs (yellow arrows) are present with an extended treatment interval (B1). At 1 week after treatment (B2), no SRF or SLGs are detected. With a shortened treatment interval (B3), SRF is slightly reduced, but the SLG appears similar to the B1 time point. A at 1 week, the next injection (B4), both SRF and SLGs have again cleared. MNV = macular neovascularization; NIR = near-infrared reflectance; SLG = subretinal lipid globules; SRF = subretinal fluid.

Despite these limitations, this study provides new and relevant clinical information and opens new opportunities for further investigations. Prospective studies determining the prevalence of these lesions over the range of both neovascular and non-neovascular AMD phenotypes could be of value. Furthermore, determining timelines of development of SLG versus SRF could serve to improve the treatment strategies for MNV due to AMD.[36]

In summary, this study broadens the location spectrum of lipid globules to include the subretinal space. We propose the term subretinal lipid globules (SLG), which refers to their content, shape, and location. Lesion composition and multimodal imaging properties, including a characteristic tail of hypertransmission, were validated through in vitro phantom experiments demonstrating a lensing effect of the SLG. However, a histological analysis is lacking to confirm the precision of the term SLG. We described the essential multimodal imaging features which differentiate SLG from other common retinal findings, including SRF. In eyes with more mature type 1 MNV, SLG may precede the detection of fluid, serving as a parameter of biological activity that could impact anti-VEGF treatment protocols.[37] Further investigation is warranted to confirm the specific composition of SLG, their relationship to choroidal caverns, and to assess their potential to serve as a clinical biomarker for disease activity.

ALL AUTHORS HAVE COMPLETED AND SUBMITTED THE ICMJE FORM FOR DISCLOSURE OF POTENTIAL CONFLICTS OF INTEREST and none were reported. This work was supported by the Macula Foundation Inc., New York, NY; National Natural Science Foundation of China award 81800879; Fundamental Research Funds of the State Key Laboratory of Ophthalmology, China, awards 2018KF04 and 2017QN05; and the Natural Science Foundation of Guangdong Province China award 2017A030310372.

D.S. is a consultant for Genentech, Heidelberg Engineering, Amgen, Bayer, Novartis, Optovue, and Regeneron. K.B.F. is a consultant for Optovue, Zeiss, Allergan, Genentech, Heidelberg Engineering, Novartis, and Roche. None of the other authors have reported any financial disclosures.

REFERENCES

1. Curcio CA, Johnson M, Rudolf M, Huang JD. The oil spill in ageing Bruch membrane. *Br J Ophthalmol* 2011;95:1638–1645.
2. Gülcan HG, Alvarez RA, Maude M, Anderson RE. Lipids of human retina, retinal pigment epithelium, and Bruch's membrane/choroid: comparison of macular and peripheral regions. *Invest Ophthalmol Vis Sci* 1993;34:3187–3193.
3. Friedman E, Smith TR. Clinical and pathological study of choroidal lipid globules. *Arch Ophthalmol* 1966;75:334–336.
4. Querques G, Costanzo E, Miere A, et al. Choroidal caverns: a novel optical coherence tomography finding in geographic atrophy. *Invest Ophthalmol Vis Sci* 2016;57:2578–2582.
5. Mullins RF, Johnson MN, Faidley EA, et al. Choriocapillaris vascular dropout related to density of drusen in human eyes with early age-related macular degeneration. *Invest Ophthalmol Vis Sci* 2011;52:1606–1612.
6. Biesemeier A, Taubitz T, Julien S, Yoeruek E, Schraermeyer U. Choriocapillaris breakdown precedes retinal degeneration in age-related macular degeneration. *Neurobiol Aging* 2014;35:2562–2573.
7. Dolz-Marco R, Glover JP, Gal-Or O, et al. Choroidal and subretinal pigment epithelium caverns. Multimodal imaging and correspondence with Friedman lipid globules. *Ophthalmology* 2018;125:1287–1301.
8. Li Y, Choi WJ, Wei W, Song S, Zhang Q, Liu J, Wang RK. Aging-associated changes in cerebral vasculature and blood flow as determined by quantitative optical coherence tomography angiography. *Neurobiol Aging* 2018;70:148–159.
9. Jacques SL. Optical properties of biological tissues: a review. *Phys Med Biol* 2013;58(11):R37–R61.
10. Pogue BW, Patterson MS. Review of tissue simulating phantoms for optical spectroscopy, imaging and dosimetry. *J Biomed Opt* 2006;11(4):041102.
11. Holladay JT. Visual acuity measurements. *J Cataract Refract Surg* 2004;30:287–290.
12. Kashani AH, Green KM, Kwon J, et al. Suspended scattering particles in motion: a novel feature of OCT angiography in exudative maculopathies. *Ophthalmol Retina* 2018;2:694–702.
13. Tuchin V. Tissue Optics. Light scattering methods and instruments for medical diagnosis. Optical Properties of Tissues With Strong (Multiple) Scattering. In: Refractive-Index Variations of Tissue. Bellingham: SPIE Press; 2007:104.
14. Michels R, Foschum F, Kienle A. Optical properties of fat emulsions. *Opt Express* 2008;16:5907–5925.
15. Boschi F, Rizzatti V, Zoico E, et al. Relationship between lipid droplets size and integrated optical density. *Eur J Histochem* 2019;25:63.
16. Tan AC, Pilgrim MG, Fearn S, et al. Calcified nodules in retinal drusen are associated with disease progression in age-related macular degeneration. *Sci Transl Med* 2018;10(466):eaat4544.
17. Coscas GJ, Lupidi M, Coscas F, Cagini C, Souied EH. Optical coherence tomography angiography versus traditional multimodal imaging in assessing the activity of exudative age related macular degeneration: a new diagnostic challenge. *Retina* 2015;35:2219–2228.
18. Kuehlewein L, Bansal M, Lenis TL, et al. Optical coherence tomography angiography of Type 1 neovascularization in age-related macular degeneration. *Am J Ophthalmol* 2015;160:739–748.
19. Xu D, Dávila JP, Rahimi M, et al. Long-term progression of type 1 neovascularization in age-related macular degeneration using optical coherence tomography. *Am J Ophthalmol* 2018;187:10–20.
20. Sarks SH. New vessel formation beneath the retinal pigment epithelium in senile eyes. *Br J Ophthalmol* 1973;57:951–965.
21. Green WR, Key SN III. Senile macular degeneration: a histopathologic study. *Trans Am Ophthalmol Soc* 1977;75:180–254.
22. Schneider U, Gelisken F, Inhoffen W, Kreissig I. Indocyanine green angiographic findings in fellow eyes of patients with unilateral occult neovascular age-related macular degeneration. *Int Ophthalmol* 1997;21:79–85.
23. Hanutsaha P, Guyer DR, Yannuzzi LA, et al. Indocyanine green video angiography of drusen as a possible predictive indicator of exudative maculopathy. *Ophthalmology* 1998;105:1632–1636.
24. Querques G, Srour M, Massamba N, et al. Functional characterization and multimodal imaging of treatment-naïve "quiescent" choroidal neovascularization. *Invest Ophthalmol Vis Sci* 2013;54:688–692.
25. Gass JD. Serous retinal pigment epithelial detachment with a notch. A sign of occult choroidal neovascularization. *Retina* 1984;4:205–220.
26. Chen L, Messinger JD, Sloan KR, et al. Nonexudative macular neovascularization supporting outer retina in age-related macular degeneration: a clinicopathologic correlation. *Ophthalmology* 2020;127(7):931–947.
27. Sarks JP, Sarks SH, Killingsworth C. Morphology of early choroidal neovascularisation in age-related macular degeneration: correlation with activity. *Eye* 1997;11:515–522.
28. Spaide RF. Optical coherence tomography angiography signs of vascular abnormalization with antiangiogenic therapy for choroidal neovascularization. *Am J Ophthalmol* 2015;160:6–16.
29. Al-Sheikh M, Iafe NA, Phasukkijwatana N, Sadda SR, Sarraf D. Biomarkers of neovascular activity in age-related macular degeneration using optical coherence tomography angiography. *Retina* 2018;38:220–230.
30. Sakurada Y, Leong BCS, Parikh R, et al. Association between choroidal caverns and choroidal vascular hyperpermeability in eyes with pachychoroid diseases. *Retina* 2018;38:1977–1983.
31. Joyal JS, Sun Y, Gantner ML, et al. Retinal lipid an glucose metabolism dictates angiogenesis though the lipid sensor Ffar1. *Nat Med* 2016;22:439–445.
32. Young SG, Zechner R. Biochemistry and pathophysiology of intravascular and intracellular lipolysis. *Genes Develop* 2013;27:459–484.
33. Casaroli-Marano RP, Peinado-ONsurbe J, Reina M, et al. Lipoprotein lipase in highly vascularized structures of the eye. *J Lipid Res* 1996;37:1037–1044.

34. Grossniklaus HE, Green WR. Choroidal neovascularization. *Am J Ophthalmol* 2004;137:496–503.
35. Freund KB, Zweifel SA, Engelbert M. Do we need a new classification for choroidal neovascularization in age-related macular degeneration? *Retina* 2010;30:1333–1349.
36. Laiginhas R, Yang J, Rosenfeld PJ, Falcão M. Nonexudative macular neovascularization - a systematic review of prevalence, natural history, and recent insights from OCT angiography. *Ophthalmol Retina* 2020;4(7):651–661.
37. Engelbert M, Zweifel SA, Freund KB. Long-term follow-up for type 1 (subretinal pigment epithelium) neovascularization using a modified "treat and extend" dosing regimen of intravitreal antivascular endothelial growth factor therapy. *Retina* 2010;30:1368–1375.